

PROPOSAL  
STUDY OF IN-MEDIUM MODIFICATION OF  $\phi$   
MESONS INSIDE THE NUCLEUS  
WITH  $\phi \rightarrow K^+K^-$  MEASUREMENT WITH THE E16  
SPECTROMETER

(Submitted to the 32nd J-PARC PAC meeting on July 14-16, 2021)

H. Sako (*spokesperson*)<sup>1,2</sup>, K. Aoki<sup>3</sup>, W. C. Chang<sup>4</sup>, M. L. Chu<sup>4</sup>, T. Chujo<sup>2</sup>,  
S. Esumi<sup>2</sup>, M. Inaba<sup>8</sup>, Y. Miake<sup>2</sup>, Y. Morino<sup>3</sup>, M. Naruki<sup>5,1</sup>, T. Nonaka<sup>2</sup>,  
K. Ozawa<sup>3,7,2</sup>, S. Sato<sup>1</sup>, T. Sakaguchi<sup>9</sup>, T. N. Takahashi<sup>6</sup>, and S. Yokkaichi<sup>6</sup>

<sup>1</sup>Advanced Science Research Center, Japan Atomic Energy Agency,  
Tokai, Ibaraki 319-1195, Japan

<sup>2</sup>Tomonaga Center for the History of the Universe,  
University of Tsukuba,  
Tsukuba, Ibaraki 305-8571, Japan

<sup>3</sup>Institute of Particle and Nuclear Studies (IPNS),  
High Energy Accelerator Research Organization (KEK),  
Tsukuba, Ibaraki 305-0801, Japan

<sup>4</sup>Institute of Physics, Academia Sinica, Taipei 11529, Taiwan

<sup>5</sup>Department of Physics, Kyoto University, Kyoto 606-8502, Japan

<sup>6</sup>RIKEN Nishina Center, RIKEN, Wako, Saitama 351-0198, Japan

<sup>7</sup>Department of Physics, University of Tokyo,  
7-3-1 Hongo, Tokyo 113-0033, Japan

<sup>8</sup>Division of Industrial Technology, Tsukuba University of Technology,  
Tsukuba, Ibaraki 305-8520, Japan

<sup>9</sup>Physics Department, Brookhaven National Laboratory,  
Upton, NY 11973-5000, USA

June 14, 2021

# Abstract

We propose to measure  $\phi \rightarrow K^+K^-$  decay in p+A collisions with the E16 spectrometer. In this measurement, we study in-medium modification of  $\phi$  properties inside the nucleus with the invariant mass spectrum and the branching ratio. This study is complementary to  $\phi \rightarrow e^+e^-$  measurement at E16, which is expected to confirm and study further the low-mass tail found in E325. In  $\phi \rightarrow K^+K^-$  decay, due to the mass close to the  $K^+K^-$  threshold, the branching ratio is sensitive to the subtle change of the  $\phi$  mass. We will measure  $\phi \rightarrow K^+K^-$  decays focusing on low velocity range, where the low-mass tail was observed in the invariant mass distribution of  $\phi \rightarrow e^+e^-$  at E325. We propose the detector configuration for the above measurements including Kaon trigger and identification using trackers, MRPCs and Aerogel Cherenkov counters. We request 30-day (90-shift) beam time to collect a few 100k  $\phi \rightarrow K^+K^-$  decays with the 30 GeV/c proton beam at the beam intensity of  $10^9$  / spill. We perform the comparison to  $\phi \rightarrow e^+e^-$  data which will be measured in Run 1, to evaluate the  $\phi$  mass modification and clarify the partial chiral symmetry restoration of  $\phi$  inside the nucleus.

---

## Contents

<b>1</b>	<b>Introduction and Goals</b>	<b>4</b>
<b>2</b>	<b>Detector Design</b>	<b>9</b>
<b>3</b>	<b>Experimental Setup</b>	<b>11</b>
3.1	Multi-gap Resistive Plate Chamber (MRPC) . . . . .	11
3.2	Track Start Counter (TSC) . . . . .	13
3.3	Aerogel Cherenkov Counter (AC) . . . . .	13
3.4	Trackers . . . . .	15
<b>4</b>	<b>Expected results</b>	<b>17</b>
<b>5</b>	<b>Beam Time Request</b>	<b>18</b>
<b>6</b>	<b>Summary</b>	<b>25</b>

# 1 Introduction and Goals

The origin of the mass of hadrons is a long standing problem. It is believed to be the chiral symmetry breaking in vacuum which leads to form quark-antiquark condensates, and the hadron in the vacuum feels constituent quark mass. In nuclear matter, hadrons are expected to change their properties due to partial chiral symmetry restoration in finite baryon density. Among various hadrons, a theoretical analysis shows the change of the  $\phi$  meson mass at finite baryon density is sensitive to the strange quark condensate [1]. The goal of the proposal is to measure the  $\phi$  meson mass inside the nucleus precisely to evaluate the strange flavor of the quark condensate.

In order to study the modification of  $\phi$  mass in the nuclear matter, we propose to measure the  $\phi \rightarrow K^+K^-$  decay in proton-nucleus (p+A) collisions, where a slow  $\phi$  is produced inside the nucleus. We measure the invariant mass spectrum and the branching ratio of the decay. Since the  $\phi$  mass is very close to the  $K^+K^-$  decay threshold, the branching ratio is expected to be sensitive to the change of  $\phi$  mass.

We will measure the  $\phi \rightarrow K^+K^-$  decay in p+A collisions at J-PARC E16. This experiment is complementary to the  $\phi \rightarrow e^+e^-$  measurement at E16. In particular, we focus on  $\phi$  mesons with low velocity, which have a large probability to stay inside the nucleus.

One of the advantages of the  $K^+K^-$  decay is that high statistics measurement is possible due to large branching ratio (49.2%) that is higher by 3 order than that of  $e^+e^-$  ( $2.973 \times 10^{-4}$ ). This makes as much more precise measurement at low  $\phi$  velocity related to in-medium modification. On the other hand, the measured invariant mass is affected by final-state interactions with nucleons inside the target nucleus, while it is not the case for the  $e^+e^-$  decay. The change of the  $\phi \rightarrow K^+K^-$  yield is furthermore influenced by the mass modifications of  $K^\pm$  inside the nucleus. It thus includes complex physics, which needs to be disentangled and understood to properly interpret the corresponding experimental data. Therefore, the formulation of theoretical models incorporating information on both  $\phi$ -N and  $K^\pm$ -N interactions will be needed. On the other hand, the  $e^+e^-$  decay is not affected by the hadronic interaction, but the statistics is limited due to the low branching ratio. In general,  $K^\pm$  decouples from the nucleus at the boundary [2] and hence the  $K^+K^-$  decay mode will show the  $\phi$  meson property at the lower density than the  $e^+e^-$  decay mode. Therefore, comparing the spectral shape difference between the two decay modes may highlight the effects of the central density. Therefore, the combination of the two decay modes will provide stringent constraints and crosschecks, which will help to clarify the  $\phi$  modification inside the nucleus.

Recently, experimental and theoretical studies on hadronic interactions have been developed using two-particle correlation measurements in high-energy heavy-ion collisions. Particularly relevant for this proposal, research for interactions of  $\phi$  and  $K$  with nucleons have been developed as follows. The LHC-ALICE experiment recently measured two-particle momentum correlation of  $p - \phi$  [3]. The analysis result shows

attractive potential between  $p$  and  $\phi$ . The result suggests mass reduction of  $\phi$  inside the nucleus, which is consistent with the observation of a low-mass tail in the  $\phi$  mass spectrum by E325. ALICE also measured the  $K^- - p$  correlation function which provides high precision data for  $K^- - p$  interaction [4]. A theoretical analysis reproduced the data successfully, based on coupled-channel potential framework [5]. These novel findings, together with other recent experimental measurements conducted at several facilities (J-PARC [6, 7], and Frascati [8]) and theoretical developments [9], will provide valuable information about the  $K^\pm$ -N interaction, which can be applied to the analysis of the data obtained from the  $K^+K^-$  decay mode.

The E325 experiment at KEK-PS [10, 11] was the prior experiment of J-PARC E16 [12], which measured  $\phi \rightarrow e^+e^-$  and  $\phi \rightarrow K^+K^-$  in p+A collisions. E325 observed a low mass tail at the  $\phi$  peak in the  $e^+e^-$  invariant mass spectrum in p+Cu collisions at low  $\phi$  velocity ( $\beta\gamma < 1.25$ ). Note that the low mass tail is observed at  $e^+e^-$  invariant mass range of  $0.94 < m_{inv} < 1.0$  GeV/ $c^2$  which is mostly below the  $\phi \rightarrow K^+K^-$  invariant mass threshold of 0.987 GeV/ $c^2$ . Therefore, the modification may appear in the  $K^+K^-$  channel more clearly than  $e^+e^-$  as the reduction of the cross section rather than the low mass tail. Indeed, no shape modification of the  $K^+K^-$  invariant mass spectra was observed in E325.

The E325 results of  $\phi \rightarrow K^+K^-$  measurement are shown in Fig. 1. The cross section of  $\phi$  is assumed to scale with the target mass number  $A$  and the  $\alpha$  parameter as,

$$\sigma_{pA}(c) = \sigma_{pp}(c)A^\alpha, \quad (1)$$

where  $c$  shows each decay channel of  $\phi \rightarrow K^+K^-$  or  $\phi \rightarrow e^+e^-$ , The  $\alpha$  parameter is obtained with C and Cu targets as follows;

$$\alpha(c) = \frac{\ln(N_c(A_1)/N_c(A_2))}{\ln(A_1/A_2)}, \quad (2)$$

and  $A_1$  and  $A_2$  is the mass numbers of Cu and C, respectively.

The difference of  $\alpha$  between  $\phi \rightarrow K^+K^-$  and  $\phi \rightarrow e^+e^-$  is related to the ratio of the two decay yields  $R = N_{K^+K^-}/N_{e^+e^-}$  as follows;

$$\Delta\alpha = \alpha(K^+K^-) - \alpha(e^+e^-) = \frac{\ln(R(A_1))/\ln(R(A_2))}{\ln(A_1/A_2)}. \quad (3)$$

If  $R(A)$  with larger  $A$  (Cu) changes with respect to that with small  $A$  (C) due to larger nuclear density effect,  $\Delta\alpha$  also changes accordingly. However,  $\Delta\alpha$  was consistent with zero (namely  $R(A)$  did not change between two targets) within statistical uncertainties, although slight increase towards low  $\beta\gamma$  was observed in the bottom right plot of Fig. 1.

However, it is clear from Fig. 1 the statistics of E325 is low, in particular at low  $\beta\gamma$ . It is therefore important to measure  $\phi \rightarrow K^+K^-$  mainly at low  $\beta\gamma$  region with large statistics.

Two strategies can be considered for  $\phi \rightarrow K^+K^-$  measurements.

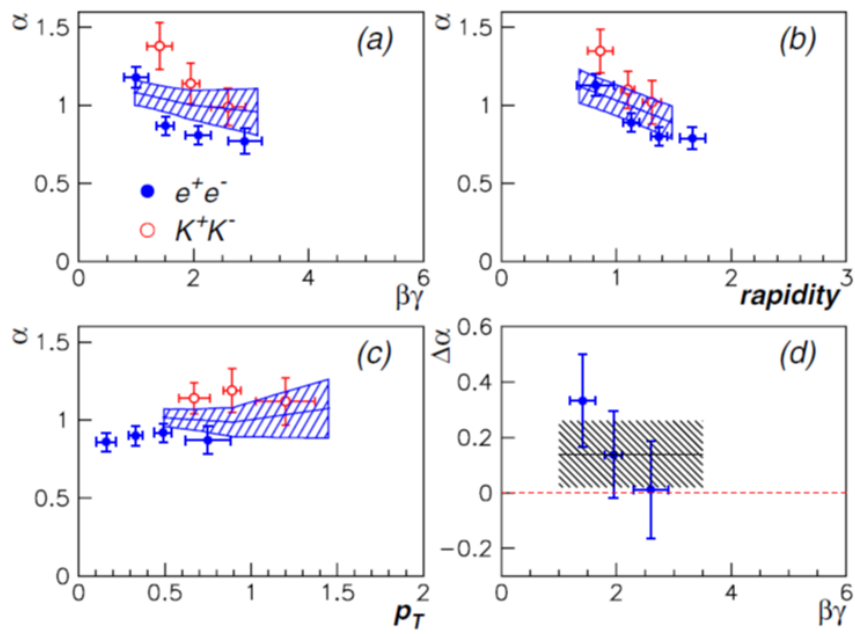


Figure 1: E325 results of  $\phi \rightarrow K^+K^-$  study are shown [11]. Top left, top right, and bottom left plots show the target nuclear dependence coefficient  $\alpha$  as a function of  $\beta\gamma$ , rapidity, and  $p_T$  of  $\phi$ . The bottom right figure shows the difference of  $\alpha$  between  $\phi \rightarrow K^+K^-$  and  $\phi \rightarrow e^+e^-$  as a function of  $\beta\gamma$ .

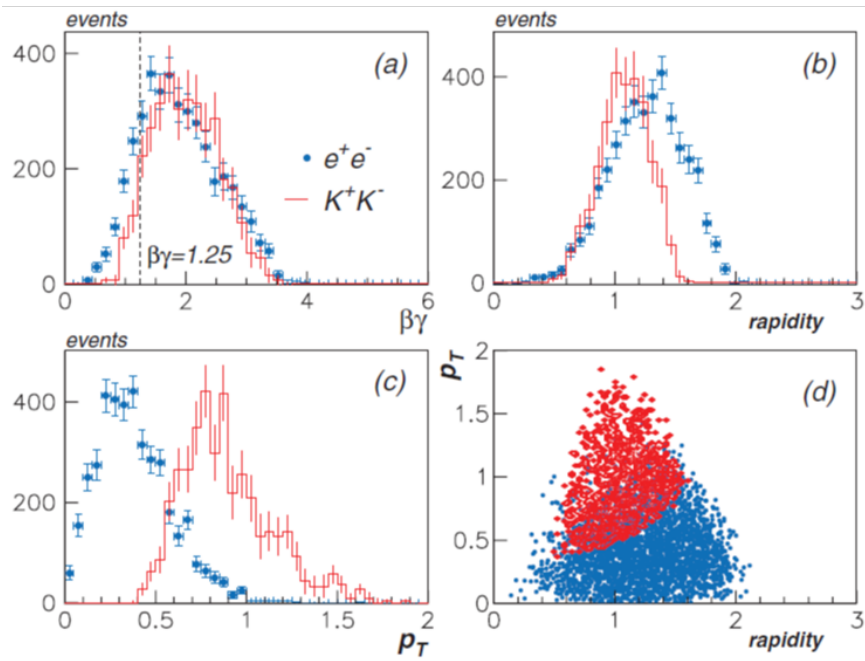


Figure 2: E325 acceptance of  $\phi \rightarrow K^+K^-$  and  $\phi \rightarrow e^+e^-$  are shown [11]. Top left, top right, and bottom left figures show acceptance in  $\beta\gamma$ , rapidity, and  $p_T$  of  $\phi$ . The bottom right figure shows the acceptance in rapidity- $p_T$ .

1. Systematic measurements in the wide  $y - p_T$  acceptance so as to have large overlap with  $\phi \rightarrow e^+e^-$ .
2. Focus on low  $\beta\gamma$  acceptance where a low mass tail in the invariant mass spectrum of  $\phi \rightarrow e^+e^-$  was observed.

In this proposal, we take Strategy 2. We use Aerogel Cherenkov counter (AC) to veto high-momentum pion background in the trigger level as shown in Fig. 3. For this strategy, we set the refractive index of the aerogel to be a large value (1.15), which is available in Japan [13], so that we enhance low  $\beta\gamma$   $\phi$  less than 1.75.

Strategy 1 is similar to that of E325, where the refractive index 1.034 was used to veto high-momentum pion background as shown in Fig. 3. E325 measured  $\phi$  in rather a wide range of  $y - p_T$  and  $\beta\gamma$ . To make larger  $y - p_T$  overlap with  $e^+e^-$  measurement, we further need to cover forward acceptance around the beam axis corresponding to the mid-rapidity. It may be good also for further systematic studies of hadron production for the physics such as small system flow, and as baseline experiments towards the future heavy-ion collision experiment at J-PARC [16]. Strategy 1 will be investigated in the future.

In this proposal, we propose to measure the  $\phi \rightarrow K^+K^-$  decay focusing on low  $\beta\gamma$ . At E325, 1.5k  $\phi \rightarrow K^+K^-$  decays were measured. We propose to collect two-order higher statistics of several-hundred-thousands to observe changes of the branching ratios between the two decay channels.

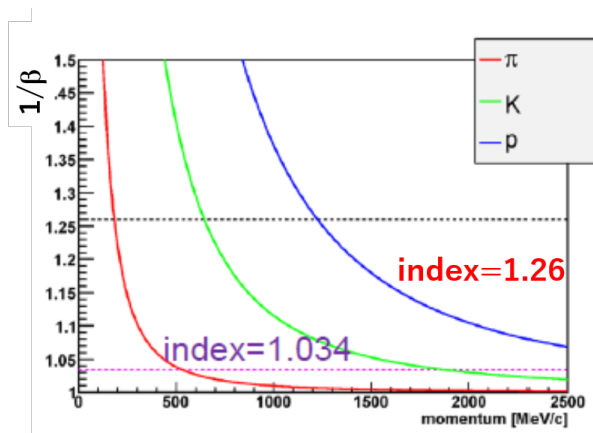


Figure 3:  $1/\beta$  as a function of the momentum for  $\pi$ ,  $K$ , and  $p$ . The refractive index of 1.034 was used for E325, whereas the proposal uses 1.15.

We consider the following two detector configurations A and B and evaluated the  $y - p_T$  acceptance using GEANT4 simulation with p+A collisions of the JAM model as shown in Figs. 5 and 6. The E16 spectrometer consists of a unit of “module”, which has the coverage in  $\theta_x$  of  $\sim 30^\circ$  and the coverage in  $\theta_y$  of  $\sim 30^\circ$ , where  $\theta_x = \tan^{-1}(x/z)$ , and  $\theta_y = \tan^{-1}(y/z)$ , and the  $z$ -,  $x$ -,  $y$ - positions are along with the beam-direction,

horizontal, and vertical directions in the left-handed coordinate system with the origin at the target.

The detector configuration and the  $y - p_T$  acceptance of  $\phi \rightarrow e^+e^-$  at Run 0 are shown in Fig. 4 where it covers the mid-rapidity of  $\sim 1.6$ .

Configurations A and B for  $\phi \rightarrow K^+K^-$  cover similar backward rapidity regions. By requiring the AC veto with the refractive index of 1.15, the acceptance is further limited to low  $p_T$  and backward rapidity as shown in Figs. 5 and 6. The  $\beta\gamma$  coverage is  $\beta\gamma < 1.75$  by requiring AC veto as shown in Fig. 7.

In this proposal, we propose Configuration A. Since the configuration does not conflict with the Run 0 detectors for  $e^+e^-$  measurements shown in Fig. 4, it is easy to install detectors with minimum interference with other existing detectors. It is also possible to perform beam tests and commissioning with beams during  $e^+e^-$  runs. In the physics runs of  $K^+K^-$ , we could run with  $e^+e^-$  measurements at the same time, while  $K^+K^-$  measurements require lower beam intensity than  $e^+e^-$ . Still a quick switch between  $K^+K^-$  and  $e^+e^-$  during the beam period will be possible.

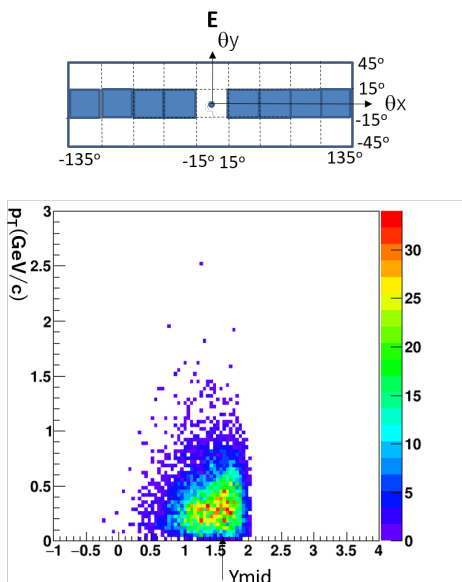


Figure 4: Detector configuration E for  $\phi \rightarrow e^+e^-$  (top) and its  $y - p_T$  acceptance (bottom) in p+C collisions.

## 2 Detector Design

The detector setup based on Configuration A is shown in Fig. 8. The E16 spectrometer consists of three vertical layers (top, middle, and bottom), and 8 modules in  $\theta_x$  [12]. In Run 0 and Run 1 setups for electron measurement, detectors are installed in the 8

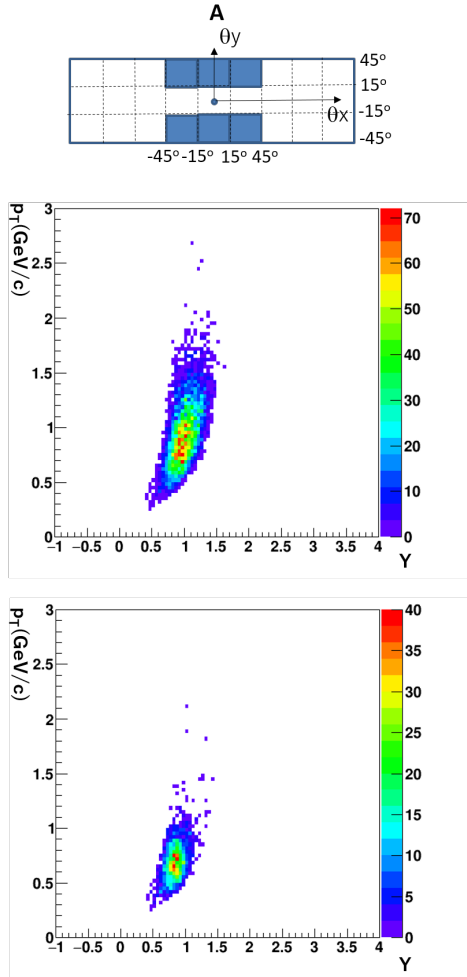


Figure 5: Detector configuration A (top), its  $y - p_T$  acceptance (middle), and the acceptance requiring AC veto with the index of 1.15 (bottom), for p+Cu collisions.

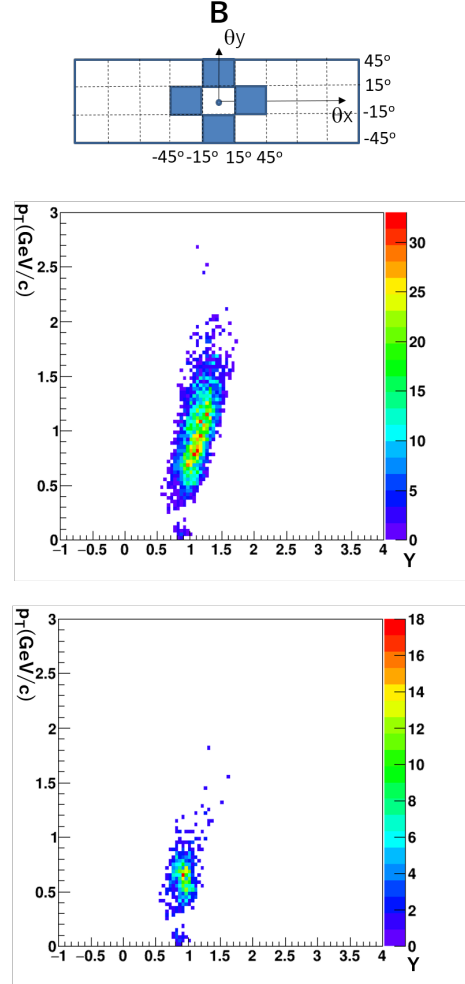


Figure 6: Detector configuration B (top), its  $y - p_T$  acceptance (middle), and the acceptance requiring AC veto with the index of 1.15 (bottom), for p+Cu collisions.

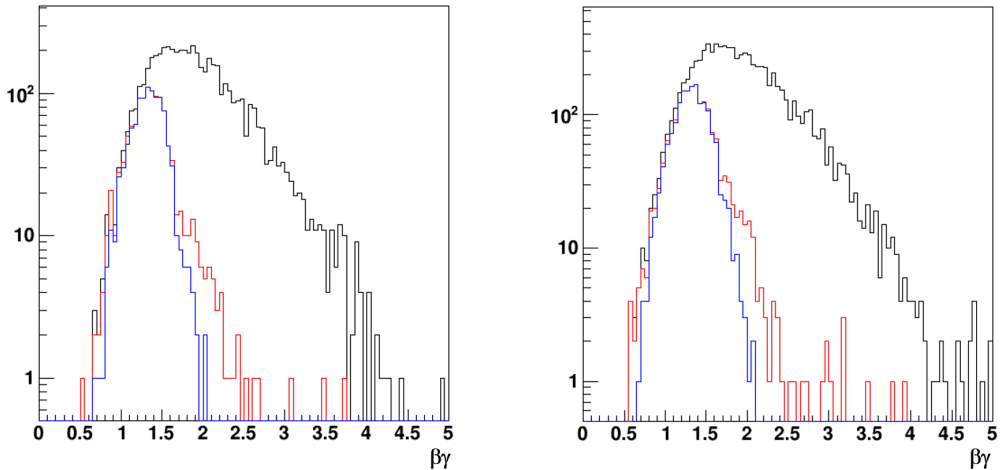


Figure 7: The  $\beta\gamma$  distributions of  $\phi$  for Configurations A for p+C (left) and p+Cu (right) collisions. The black lines are without selection, red lines are with AC veto, and blue lines are with the unlike-sign track trigger described below.

modules in the middle layer [17]. For charged particle tracking, the Silicon Strip Detectors (SSDs), three-layer GEM trackers (GTRs) are used. For electron identification, Hadron Blind Detectors (HBD) and Lead-glass Calorimeter (LG) are used.

We use only the top and bottom layers in Configuration A. In the top and bottom layers, we use GTRs in the 6 most-forward modules for A to cover the horizontal angle range of  $-45^\circ < \theta_x < 45^\circ$ . We will install the start timing counters (Track Start Counter, TSC) at  $R \sim 0.1$  m, Aerogel Cherenkov Counters (AC) at  $R \sim 1.1$  m, and MRPCs at  $R \sim 1.3$  m.

In the following subsections, the detector design and prototype R&D status of the new detector for  $\phi \rightarrow K^+K^-$  measurements will be described.

## 3 Experimental Setup

### 3.1 Multi-gap Resistive Plate Chamber (MRPC)

In order to identify charged Kaons, MRPC is used for high-resolution time-of-flight measurement. Fig. 9 shows the expected particle identification performance assuming the TSC and MRPC timing resolution of 50 ps and 60 ps with the path length of 1.2 m, respectively. We are developing an MRPC based on that of BGOegg experiment [18]. The structure of the MRPC is shown in Fig. 10. It consists of an anode PCB in the middle, and cathode PCBs in the top and bottom. Between top and bottom cathode PCBs, there are 10 gas gap of  $120 \mu\text{m}$  made of 12 sheets of glass with plastic strings as spacer. About  $\pm 7\text{kV}$  is applied on the top and bottom cathode electrodes while the anode electrode is grounded so that electron avalanche is produced

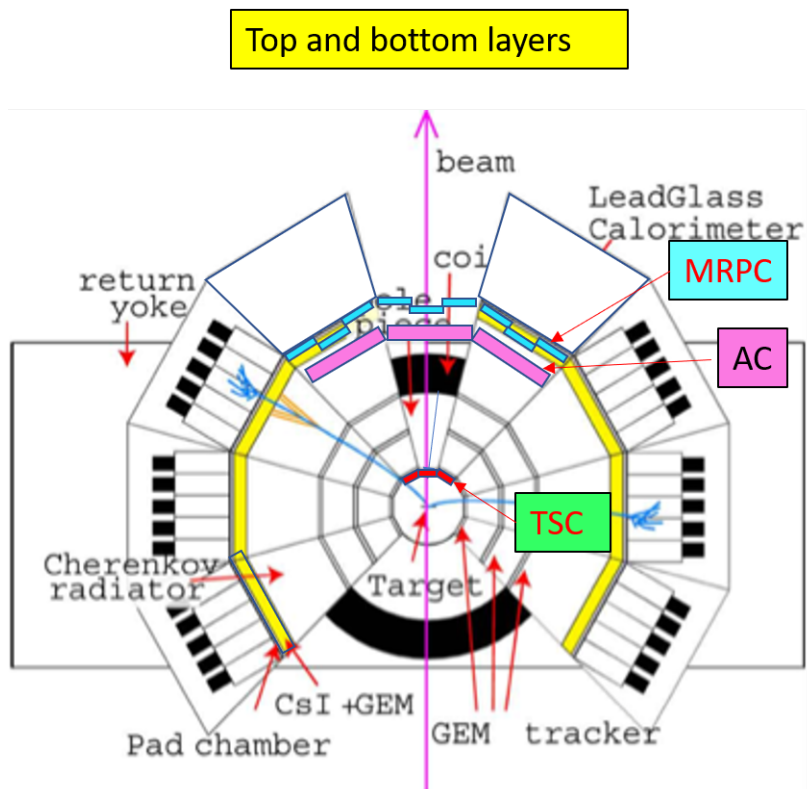


Figure 8: The detector setup in Configuration A in the top and bottom layers. AC denotes the Aerogel Cherenkov Counters, and TSC denotes Track Start Counters.

in the gas gaps when a charge particle passes through. The electrodes are made of high-resistive carbon sheets. The MRPC has 8 readout strips in the anode PCB with the dimension of  $26\text{mm} \times 770\text{mm}$  as shown in Fig. 11. We constructed a prototype MRPC and tested it with LEPS beamline in Nov. 2020. In the preliminary analysis we obtained the detector efficiency of more than 90% and the timing resolution of 72 ps with slewing corrections, respectively. The resulting TOF resolution and TOF vs time-over-threshold correlation are shown in Fig. 13 and 14.

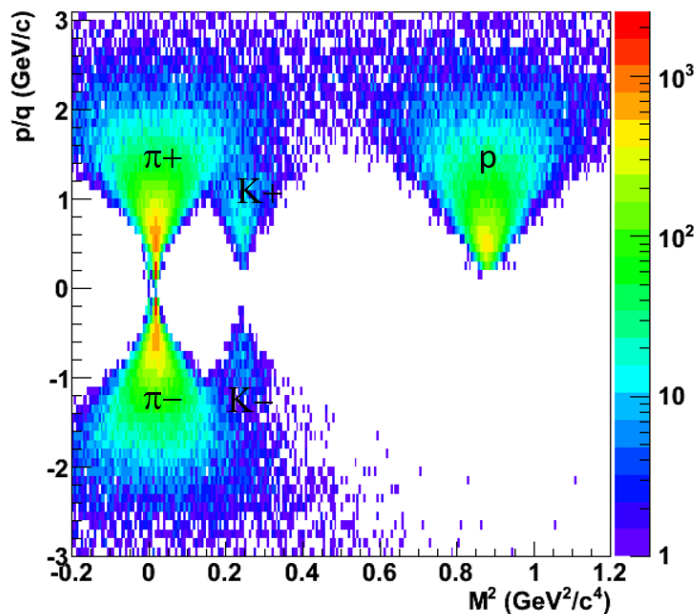


Figure 9: Simulated rigidity ( $\text{GeV}/c$ ) as a function of squared mass ( $\text{GeV}^2/c^2$ ) assuming the TSC and MRPC timing resolution of 50 ps and 60 ps with the path length of 1.2 m, respectively.

### 3.2 Track Start Counter (TSC)

Track Start Counter (TSC) is the start timing counter for the time-of-flight measurement with MRPC, which is a segmented plastic scintillation counter. A prototype TSC consists of 8 segments of  $4\text{ mm} \times 4\text{ mm} \times 100\text{ mm}$  plastic scintillator, where scintillation light is detected with MPPC with  $3\text{ mm} \times 3\text{ mm}$  sensitive area. In the test with a beta-ray source, we obtained the timing resolution of  $55 \pm 5$  ps.

### 3.3 Aerogel Cherenkov Counter (AC)

Aerogel Cherenkov Counter (AC) is used to veto fast pion background in the trigger. The AC prototype was developed with the aerogel radiator with the refractive index of 1.034, with fine-mesh PMT of 3-inch diameter for photon detection. Since AC is

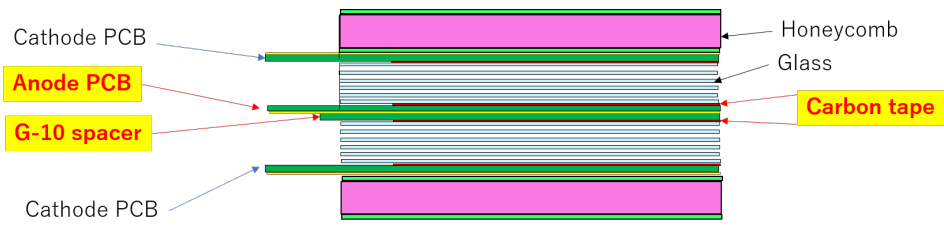


Figure 10: The MRPC structure.

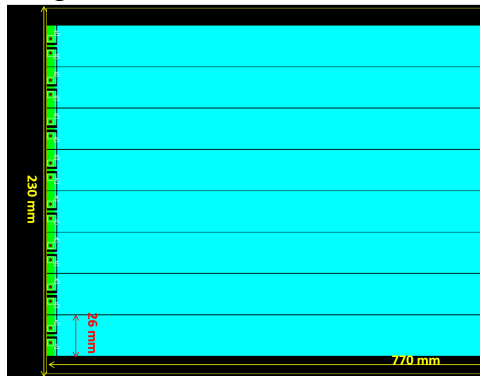


Figure 11: The MRPC anode PCB design.

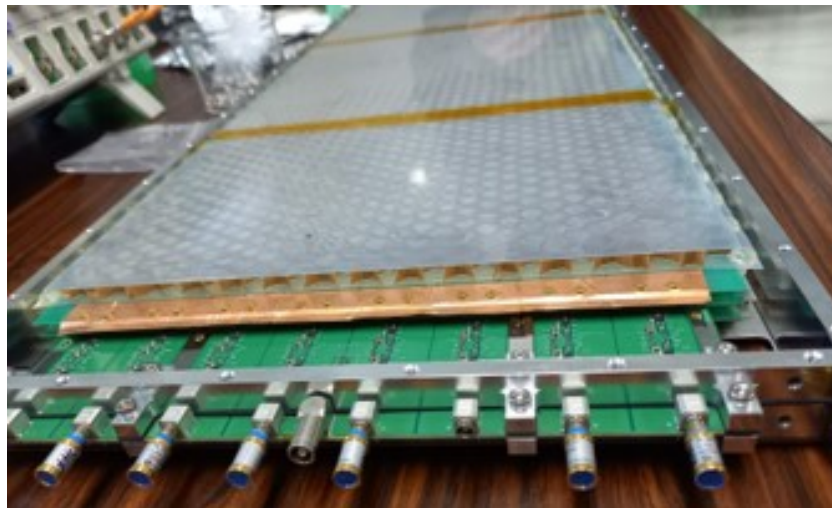


Figure 12: A photograph of an MRPC prototype.

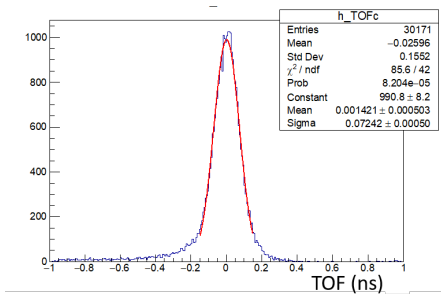


Figure 13: The measured TOF distribution of electron beams of light velocity with an MRPC.

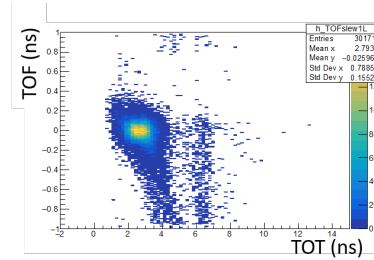


Figure 14: The measured TOF in an MRPC as a function of Time-Over-Threshold (TOT) of electron beams.

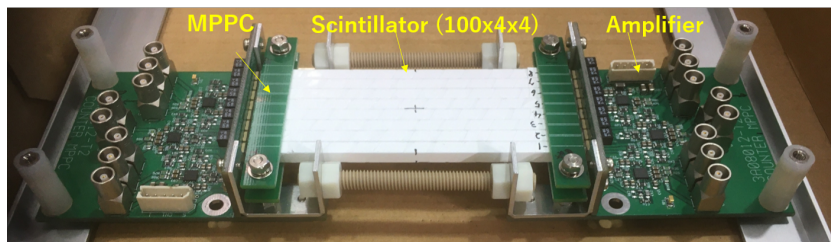


Figure 15: A photograph of a TSC prototype.

used inside the magnetic field of the E16 spectrometer, a fine-mesh PMT is required. Its design and photograph is shown in Figs. 16 and 17 [19].

For this proposal, we will modify the design. First, we will change the aerogel radiator with the refractive index of 1.15. The variety of the index is available which have been produced at Chiba University [13, 14, 15]. A pin hole drying method is used to produce high index aerogel up to 1.26, which has good transparency. We also change the direction of the PMTs to the vertical direction to minimize the effect of the fringe magnetic field. The radiator area of one AC module will be 120 ( $x$ )  $\times$  400 mm ( $y$ ) which faces to the target direction. The dimension is chosen to reduce the overkilling effect within 10%. We will use two vertical direction fine-mesh PMTs for one unit, and the Cherenkov photons will be reflected 90° with curved mirrors which focus the photons onto the PMT windows.

### 3.4 Trackers

In the top and bottom layers, we adopt SSDs and GTRs as tracking devices which are used for electron measurements at E16 [12, 20, 21].

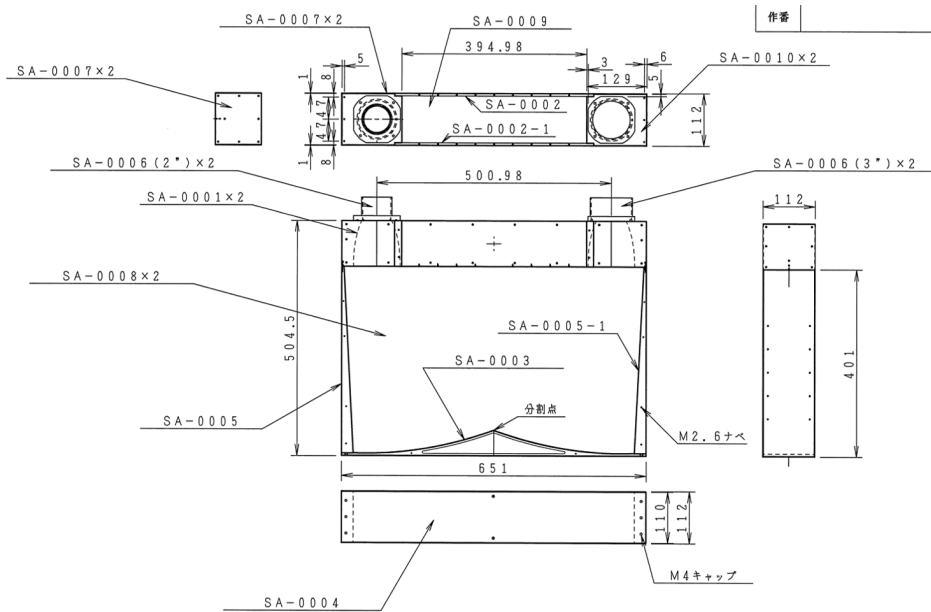


Figure 16: The design of the AC prototype.

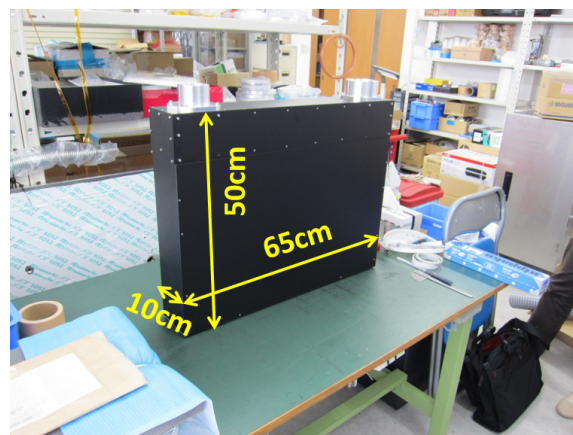


Figure 17: A photograph of the AC prototype.

## 4 Expected results

We describe here the definition of the triggers, and evaluate the performance of the trigger, Kaon identification, and the invariant mass spectra of  $K^+K^-$  in the simulation.

We define the triggers as below, based on those used in E325. The “Unlike-sign” trigger is to select two unlike-charge particles and reject high-momentum charge particles using TSC slat and MRPC strip information. The “ $KK$ ” trigger is to select  $K^+K^-$ .

### 1. Unlike-sign trigger

- (a) Require at least 2 MRPC hits with AC veto
- (b) Require at least two fast charged tracks in the matrix of MRPC strip ID and TSC slat ID as shown in Fig. 19.
- (c) At least one pair of fast tracks with opposite charge

### 2. $KK$ trigger

- (a) Cut using the relation among the time of flight (TOF) between TSC and MRPC, TSC slat ID, and MRPC strip ID to select tracks consistent with  $K^\pm$ , as shown in Fig. 23.
- (b) Require at a pair of  $K^\pm$  candidate tracks

We use AC with the refractive index of 1.15. The inverse of the velocity as a function of momentum is shown in Fig. 3. The momentum threshold above which Cherenkov light is emitted is about 0.2 GeV/c, 0.6 GeV/c, and 1.2 GeV/c for  $\pi$ ,  $K$ , and  $p$ , respectively. We assume the AC efficiency to be 90 % above the velocity threshold of 0.794, and 8 % below the threshold, which are the values of the E325 AC.

Fig. 18 shows the horizontal hit position  $R\theta_x$  of MRPC as a function of that of TSC with AC vetoed tracks, where  $R = \sqrt{x^2 + z^2}$  and  $\theta = \tan^{-1}(x/z)$ . It includes the information of both the initial track angle and the deflection depending on its momentum.

In order to suppress the effect of the initial track angle, we redefine a variable which is a measure of the track deflection as;

$$\Delta R\theta_x = R\theta_x(\text{MRPC}) - aR\theta_x(\text{TSC}), \quad (4)$$

where Parameter  $a$  is obtained by the straight-line fit to the proton distribution.

The resulting horizontal track deflection  $\Delta R\theta_x$  is shown in Fig. 19. It is flat as a function of the TSC position. To reject tracks with small position deflection (namely high momentum), we apply the cut shown as red boxes.

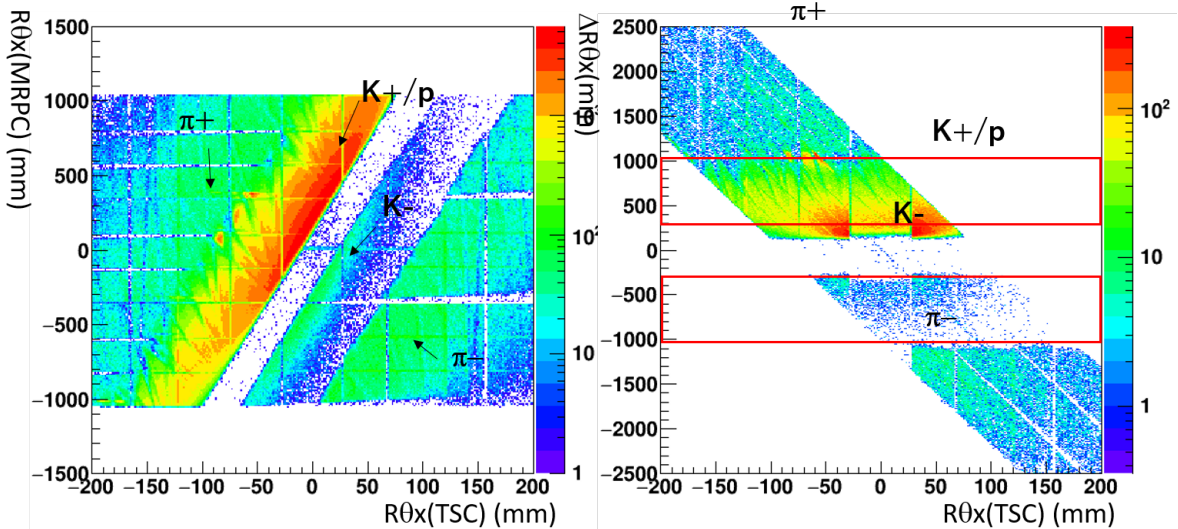


Figure 18: The horizontal hit position  $R\theta_x$  of MRPC as a function of that of TSC for all of the particles.

Figure 19: The horizontal track deflection  $\Delta R\theta_x$  of MRPC as a function of the TSC horizontal hit position  $R\theta_x$  for all of the particles. The red triangles denote the fast particle selection cut.

The cuts are determined by looking at  $\Delta R\theta_x$  for each particle shown in Figs. 20, 21, and 22. The plots reflect the track position deflection from TSC to MRPC depending on their rigidity distributions.  $\pi$  has larger  $\Delta R\theta_x$  than  $K$  and  $p$ , due to lower momentum with AC veto.

The Kaon selection trigger using the relation between  $\Delta R\theta_x$  and TOF between TSC and MRPC is simulated in Fig. 23. The Kaon selection cut is defined as the two parallelograms, which is used for the  $KK$  trigger selection.

Figs. 24 and 25 show the invariant mass spectra in p+C and p+Cu simulated in GEANT4 with the JAM model, after the trigger selections described above. The momentum and angle resolution due to detector resolution and multiple scattering is included. These plots include background due to mis-identified Kaons due to finite AC efficiency.

## 5 Beam Time Request

The request for the beam time and beam conditions is summarized in Table 1. We request 30 days (90 shifts) as the beam time for this proposal. The beam condition is the 30 GeV proton beam at the beam rate of  $10^9$  protons / spill. We will obtain a few hundred thousands  $\phi \rightarrow K^+K^-$  decays, which are 2-order more than the statistics of E325. We request dedicated beam time separate from the  $\phi \rightarrow e^+e^-$  run such as

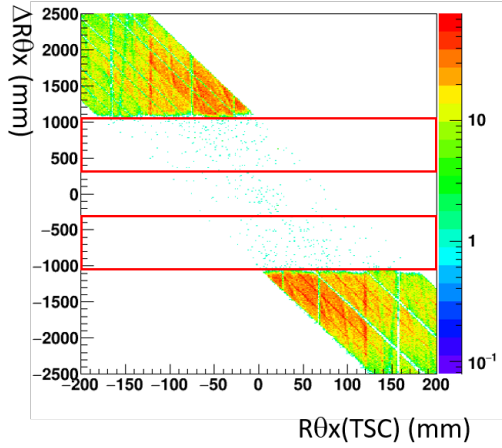


Figure 20: The horizontal track deflection  $\Delta R\theta_x$  with AC veto as a function of the horizontal hit position of TSC  $R\theta_x$  for  $\pi^\pm$ .

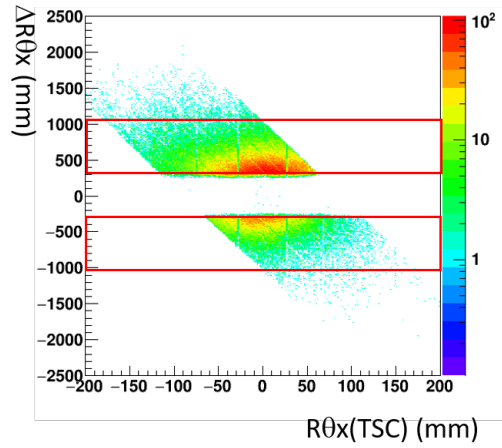


Figure 21: The horizontal track deflection  $\Delta R\theta_x$  with AC veto as a function of the horizontal hit position of TSC  $R\theta_x$  for  $K^\pm$ .

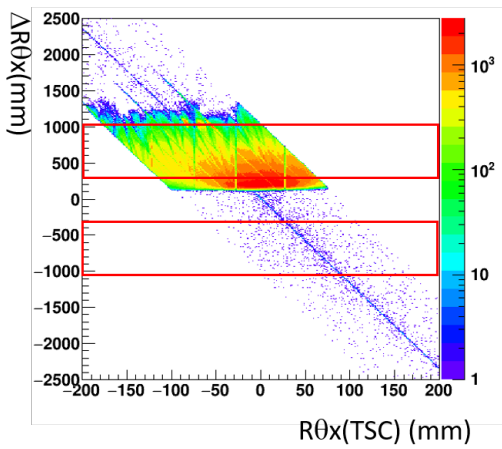


Figure 22: The horizontal track deflection  $\Delta R\theta_x$  with AC veto as a function of the horizontal hit position of TSC  $R\theta_x$  for  $p$ .

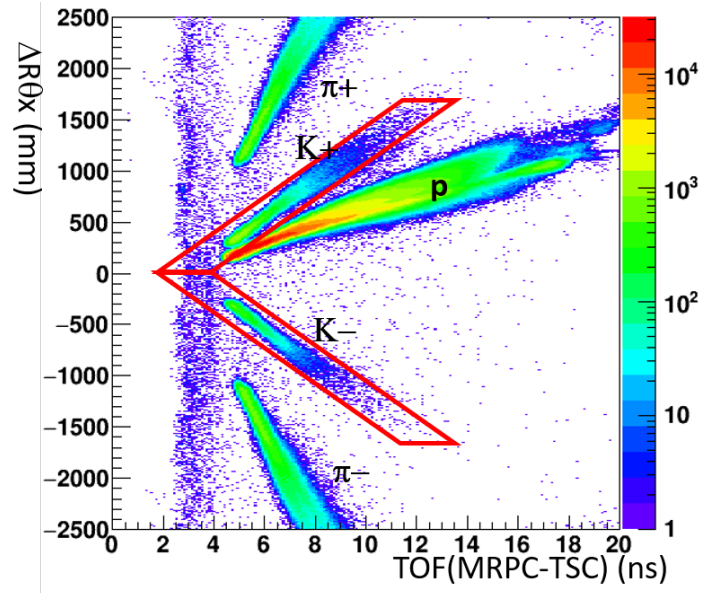


Figure 23: The corrected hit position in  $R\theta$  of MRPC as a function of TOF between TSC and MRPC. The red parallelograms denote Kaon selection cut.

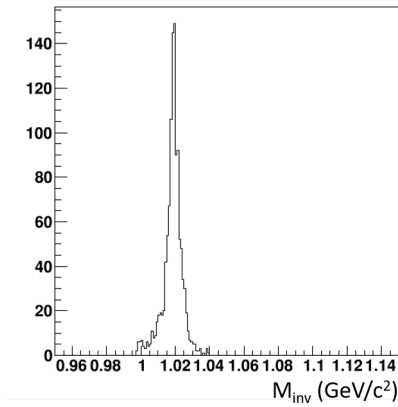


Figure 24: The invariant mass spectrum of  $K^+K^-$  with  $1M \phi \rightarrow K^+K^-$  decay JAM events in p+C.

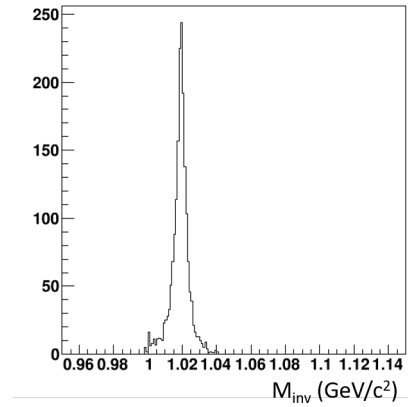


Figure 25: The invariant mass spectrum of  $K^+K^-$  with  $1M \phi \rightarrow K^+K^-$  decay JAM events in p+Cu.

E16 Run 1, since the proposed experiment requires the lower-intensity beam of  $10^9$  / spill than that of  $\phi \rightarrow e^+e^-$  runs ( $10^{10}$  / spill). The lower beam intensity for the  $\phi \rightarrow e^+e^-$  measurement is due to the limited rate capability of MRPCs and the DAQ rate of  $\sim 1$ kHz.

Below, we will show estimation of the statistics of  $\phi \rightarrow K^+K^-$  decays, and the statistical errors. We will show also the comparison to  $\phi \rightarrow e^+e^-$  data which will be collected in E16 Run 1.

Table 1: The beam time and the beam condition requests for this proposal.

Beam line	High-momentum beam line
Beam time	30 days (90 shifts)
Beam particle	proton
Beam momentum	30 GeV/c
Beam intensity	$10^9$ / spill

Trigger rates and true  $\phi \rightarrow K^+K^-$  rates per p+A collision event in GEANT4 simulation with JAM model are summarized in Table 2 in p+C and p+Cu for Configuration A.

Table 2: The trigger rates and true  $\phi \rightarrow K^+K^-$  rates per p+A collision in Configuration A in p+C and p+Cu estimated from JAM event generator and GEANT4 simulation. No contribution from beam halo is included.

	p+C	p+Cu
Unlike-sign Trigger	$(1.1 \pm 0.1) \times 10^{-3}$	$(3.8 \pm 0.1) \times 10^{-3}$
$KK$ trigger	$(3.1 \pm 0.3) \times 10^{-5}$	$(6.1 \pm 0.3) \times 10^{-5}$
$\phi \rightarrow K^+K^-$	$(1.2 \pm 0.2) \times 10^{-5}$	$(2.0 \pm 0.2) \times 10^{-5}$

In order to estimate the expected  $\phi \rightarrow K^+K^-$  yield, we use the parameters summarized in Table. 3. We assume to use the common C and Cu targets for E16 Runs 0 and 1 [17].

In E325, there was a factor of 10 higher first-level trigger rate than that estimated in the simulation, which is attributed to the background tracks due to beam halo. Since we use the proton beam rate of  $1 \times 10^9$  per spill, and the target interaction rate of 0.1%, the  $KK$  trigger rate is 61 for p+Cu. Even if we consider the above enhancement factor of 10, it is well below the DAQ limit of 1kHz.

We estimated the inefficiency of the overkilling effect that is the Kaon veto fails due to a fast particle above AC threshold hits the same AC module at the same time using GEANT4 simulation with JAM event generator. Using the size of the AC module of  $120$  ( $x$ )  $\times$   $400$  mm ( $y$ ), the efficiency loss can be suppressed to less than 10%.

Table 3: The parameters used to estimate  $\phi \rightarrow K^+K^-$  statistics.

Parameter	p+C	p+Cu	Note
$\phi$ cross section (mb)	1.2	4.8	E16 Run0 proposal [17]
Branching ratio of $\phi \rightarrow K^+K^-$		0.492	PDG 2018
Target thickness (atom/cm <sup>2</sup> )	$4.55 \times 10^{21}$	$1.35 \times 10^{21}$	E16 Run0 proposal [17]
Protons per spill		$1 \times 10^9$	spill = 2 sec duration
Spills per hour		652	5.52 sec MR cycle
Beam available time		70%	Downtime of beam, DAQ, calib.
DAQ live time		76%	E16 Run0 proposal [17]
Trigger efficiency		70%	Unlike-sign and $KK$ triggers
Detector acceptance	0.11%	0.17%	Including AC veto of track pair
Pair reconstruction eff.		70%	E16 Run0 proposal [17]
MRPC eff.		73%	For pair track
AC overkilling effect	100%	90%	Estimated from simulation

Then, we estimated  $\phi \rightarrow K^+K^-$  yields in 30-day (160-shift) beam time time with Configuration A as shown in Tables 4. We assume the proton beam rate to be  $1 \times 10^9$  per spill, which is 10 times lower than the beam rate for  $\phi \rightarrow e^+e^-$  of  $1 \times 10^{10}$ , considering the maximum DAQ rate and the rate capability of MRPCs.

The  $\phi \rightarrow e^+e^-$  yields expected E16 Run 1 in 160 shifts described in E16 Run0 Proposal [17] are also shown in the table. The estimation is based on the parameter table (Table II) in the proposal. We performed GEANT4 simulation with JAM event generator to estimate the yields in the two low  $\beta\gamma$  bins ( $\beta\gamma < 1.25$ , and  $1.25 \leq \beta\gamma < 1.75$ ). At these  $\beta\gamma$  ranges, there is some  $y - p_T$  overlap between  $\phi \rightarrow K^+K^-$  and  $\phi \rightarrow e^+e^-$  as shown in Figs. 26 and 27. We used the cut in the plots as shown in black lines to estimate the overlap fraction of  $K^+K^-$  and  $e^+e^-$  yields and also showed in the table. The fraction for  $K^+K^-$  is more than 80% while that for  $e^+e^-$  is less than 10%.

From these data, we estimated the expected relative statistical errors of  $\alpha$  parameter of the target nucleus dependence of the  $\phi$  production cross section (Eq. 3), used in the E325 paper in Table 5. In the  $y - p_T$  overlap region, a direct comparison of the  $K^+K^-$  and  $e^+e^-$  yields is possible to evaluate the ration of the branching ratios. It was not done in E325. We showed the relative statistical uncertainties for that also in the table.

The statistical error of  $\alpha$  will be improved significantly for  $K^+K^-$  and slightly for  $e^+e^-$  compared to E325 as shown in Fig. 28.

Also the direct measurement of the branching ratio of  $\text{BR}(\phi \rightarrow K^+K^-)/\text{BR}(\phi \rightarrow e^+e^-)$  will be done in the  $y - p_T$  overlap region with the uncertainties of 7-10%.

Table 4: Expected  $\phi \rightarrow K^+K^-$  yields in p+C and p+Cu for 30-day run with Configuration A, and expected  $\phi \rightarrow e^+e^-$  yields in p+C and p+Cu for 160-shifts in E16 Run1.

	$\phi \rightarrow K^+K^-$		$\phi \rightarrow e^+e^-$	
	p+C	p+Cu	p+C	p+Cu
Total	159k	262k	12.5k	14.8k
$\beta\gamma < 1.25$	72k	113k	1.4k	1.8k
$1.25 < \beta\gamma < 1.75$	84k	146k	2.3k	3.0k
Overlap $y - p_T$ ( $\beta\gamma < 1.25$ )	65k	100k	98	150
Overlap $y - p_T$ ( $1.25 < \beta\gamma < 1.75$ )	83k	143k	130	180

Table 5: Expected relative statistical uncertainties for the  $\alpha$  parameter with p+C and p+Cu data for  $\phi \rightarrow K^+K^-$  and for  $\phi \rightarrow e^+e^-$ , and expected relative statistics uncertainties for the BR ratio at  $y - p_T$  overlap region for p+C and p+Cu collisions.

Relative error of $\alpha$	$\phi \rightarrow K^+K^-$	$\phi \rightarrow e^+e^-$
Total	0.51%	2.3%
$\beta\gamma < 1.25$	0.78%	6.4%
$1.25 \leq \beta\gamma < 1.75$	0.68%	4.9%
Relative error of BR ratio	p+C	p+Cu
Total	6.7%	5.5%
$\beta\gamma < 1.25$	10%	8.2%
$1.25 \leq \beta\gamma < 1.75$	8.9%	7.4%

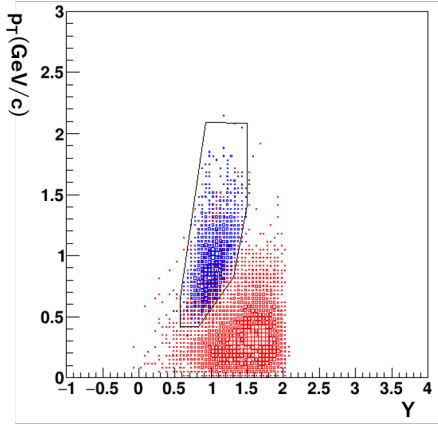


Figure 26: The  $y$ - $p_T$  acceptance of  $K^+K^-$  in Configuration A (blue) and  $e^+e^-$  for Run 1 configuration (8 modules) (red) in p+C JAM events.

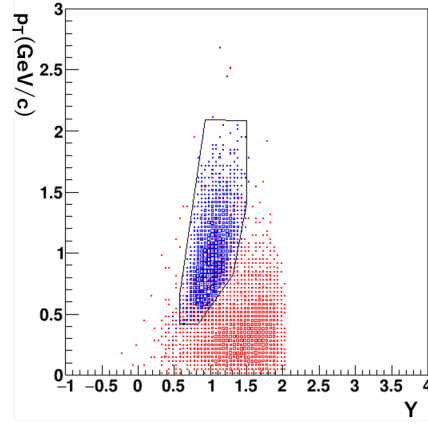


Figure 27: The  $y$ - $p_T$  acceptance of  $K^+K^-$  in Configuration A (blue) and  $e^+e^-$  for Run 1 configuration (8 modules) (red) in p+Cu JAM events.

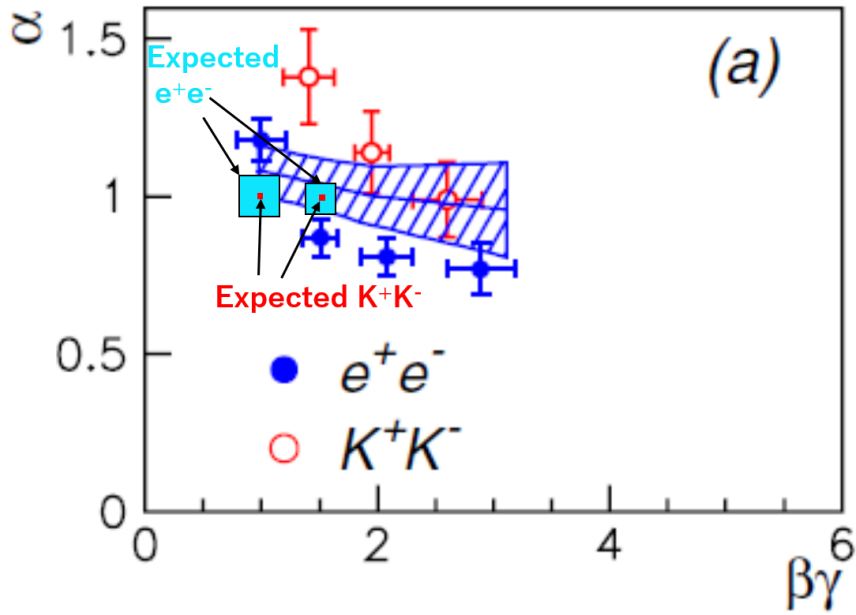


Figure 28: Expected statistical uncertainties of the  $\alpha$  parameter for  $K^+K^-$  (red small squares) in this proposal and  $e^+e^-$  in Run 1 (cyan squares) are shown at  $\beta\gamma < 1.25$  and  $1.25 \leq \beta\gamma < 1.75$ . The vertical size of each square corresponds to  $2\sigma$  of the statistical error.

## 6 Summary

We propose to study modification of  $\phi$  mass inside the nucleus, which is related to partial chiral symmetry restoration, through  $\phi \rightarrow K^+K^-$  measurements with the E16 spectrometer. We will measure invariant spectra and branching ratios of  $K^+K^-$  in 2-order higher statistics than KEK-E325. This study is complementary to  $\phi \rightarrow e^+e^-$  measurements at J-PARC E16, and E325, where a low-mass tail at the  $\phi \rightarrow e^+e^-$  peak in the invariant mass spectrum was observed at low  $\phi$  velocity in p+Cu. We propose to measure  $\phi \rightarrow K^+K^-$  yields in the horizontal angles from  $-45^\circ$  to  $45^\circ$  in the top and bottom layers. We introduce Kaon identification detectors, Aerogel Cherenkov counter, MRPC and the start counter (TSC), and build trackers for these measurements. For the proposed experiment, we request the beam time of 30 days (90 shifts), with the 30 GeV proton beam at the beam rate of  $10^9$  protons / spill. Since the required beam rate is lower than the  $\phi \rightarrow e^+e^-$  experiment, we request separate beam time. We expect to collect 160k and 260k  $\phi \rightarrow K^+K^-$  decays in p+C and p+Cu collisions in 30-day beam time. We reduce the statistical uncertainties of the  $\alpha$  parameter at  $\beta\gamma < 1.75$  by more than 1 order compared to E325, and also the direct measurement of the branching ratio of  $\text{BR}(\phi \rightarrow K^+K^-)/\text{BR}(\phi \rightarrow e^+e^-)$  will be carried out in the  $y - p_T$  overlap region with the uncertainties of 7-10%. These measurements may contribute to establishing the mass modification of  $\phi$  in the nucleus experimentally as well as to unveiling the relation to partial chiral symmetry restoration.

## References

- [1] P. Gubler and K. Ohtani, *Phys. Rev. D* **90** 094002 (2014)
- [2] HADES Collaboration, *Phys. Lett. B* **778** 403 (2018)
- [3] ALICE Collaboration, arXiv:2105.05578.
- [4] S. Acharya *et al.* (ALICE Collaboration), *Phys. Rev. Lett.* **124** 092301 (2020)
- [5] Y. Kamiya *et al.*, *Phys. Rev. Lett.* **124** 132501 (2020)
- [6] T. Yamaga *et al.*, *Phys. Rev. C* **102** 044002 (2020)
- [7] Y. Ichikawa *et al.*, *Prog. Theo. Exp. Phys.* **2015** 021D01 (2015)
- [8] M. Bazzi *et al.*, *Phys. Lett. B* **704** 113 (2011)
- [9] Y. Ikeda *et al.*, *Phys. Lett. B* **706** 63 (2011)
- [10] R. Muto *et al.*, *Phys. Rev. Lett.* **98** (2007) 042501.
- [11] F. Sakuma *et al.*, *Phys. Rev. Lett.* **98** (2007) 152302.
- [12] S. Yokkaichi *at al.*, J-PARC proposal No. 16 [http://j-parc.jp/researcher/Hadron/en/pac\\_0606/pdf/p16-Yokkaichi\\_2.pdf](http://j-parc.jp/researcher/Hadron/en/pac_0606/pdf/p16-Yokkaichi_2.pdf), *Lec. Notes. Phys.* **781** (2009) 161-193.
- [13] M. Tabata, <http://jahep.org/hepnews/2019/19-4-3-aerogel.pdf> (in Japanese).
- [14] M. Tabata, *Phys. Procedia* **37** 642-649 (2011).
- [15] M. Tabata, *JPS Conf. Proc.* **8** 022004 (2015).
- [16] H. Sako, *et al.*, Letter-Of-Intent of J-PARC-HI, [https://j-parc.jp/researcher/Hadron/en/pac\\_1607/pdf/LoI\\_2016-16.pdf](https://j-parc.jp/researcher/Hadron/en/pac_1607/pdf/LoI_2016-16.pdf).
- [17] S. Yokkaichi *at al.*, J-PARC E16 Run0 Proposal, [http://j-parc.jp/researcher/Hadron/en/pac\\_1707/pdf/E16\\_2017-10.pdf](http://j-parc.jp/researcher/Hadron/en/pac_1707/pdf/E16_2017-10.pdf).
- [18] N. Tomida *et al.*, *JINST* **11** C11037 (2016).
- [19] F. Sakuma, E16 internal presentation in Aug. 2011.
- [20] R. Kiuchi, *et al.*, *Nucl. Instrum. Meth. A* **763**, 399-403 (2014).
- [21] K. Komatsu, *et al.*, *Nucl. Instrum. Meth. A* **732**, 241-244 (2013).